Targeted Deletion of the PEX2 Peroxisome Assembly Gene in Mice Provides a Model for Zellweger Syndrome, a Human Neuronal Migration Disorder

Phyllis L. Faust and Mary E. Hatten

Laboratory of Developmental Neurobiology, The Rockefeller University, New York, New York 10021

Abstract. Zellweger syndrome is a peroxisomal biogenesis disorder that results in abnormal neuronal migration in the central nervous system and severe neurologic dysfunction. The pathogenesis of the multiple severe anomalies associated with the disorders of peroxisome biogenesis remains unknown. To study the relationship between lack of peroxisomal function and organ dysfunction, the *PEX2* peroxisome assembly gene (formerly peroxisome assembly factor-1) was disrupted by gene targeting.

Homozygous *PEX2*-deficient mice survive in utero but die several hours after birth. The mutant animals do not feed and are hypoactive and markedly hypotonic. The *PEX2*-deficient mice lack normal peroxisomes but do assemble empty peroxisome membrane ghosts. They display abnormal peroxisomal biochemical parameters, including accumulations of very long chain fatty acids in plasma and deficient erythrocyte plasmalogens. Abnormal lipid storage is evident in the adrenal cortex, with characteristic lamellar–lipid inclusions. In the central nervous system of newborn mutant mice there is disordered lamination in the cerebral cortex and an increased cell density in the underlying white matter, indicating an abnormality of neuronal migration. These findings demonstrate that mice with a *PEX2* gene deletion have a peroxisomal disorder and provide an important model to study the role of peroxisomal function in the pathogenesis of this human disease.

NEURONAL migration disorders are a diverse group of human brain malformations that primarily affect development of the cerebral cortex. Over 25 syndromes with abnormal neuronal migrations have been described and many have been proven to be genetic in origin (Dobyns and Truwit, 1995). Classical studies on the formation of cortical architecture in human brain have revealed four basic steps, including neuronal precursor proliferation in germinal zones, directed migration from germinal zones, assembly of postmigratory cells into discrete layers, and the formation of synaptic connections. The migration of immature cortical neurons on a scaffold of radial glial cells during mid to late gestation is a remarkable feature of cortical formation (Rakic, 1972; Hatten, 1990), providing mechanisms for the disposition of different classes of neurons into specific neuronal layers. While attention has focused on neuron–glia interactions during neuronal locomotion on glial fibers (Zheng et al., 1996), cell organelles such as the peroxisome, which function in cellular metabolism, are also critical to this process.

Zellweger syndrome is a severe, autosomal recessive human neuronal migration disorder. It is a prototype for peroxisome biogenesis disorders (PBDs)[1] in which the organelle is not correctly assembled, leading to multiple defects in peroxisome function (Lazarow and Moser, 1994). These infants are readily recognized in the early postnatal period by their characteristic dysmorphic facial features, profound generalized hypotonia, psychomotor delay, and seizures. There is progressive dysfunction of the liver and central nervous system, culminating in death within the first year of life. Morphologic changes are present in multiple organ systems including central nervous system malformations, renal cysts, hepatic fibrosis, joint calcifications, striated adrenocortical cells (Goldfischer et al., 1973), and ocular abnormalities. The clinical spectrum of PBDs also includes the milder disorders neonatal adrenoleukodystrophy (NALD) and infantile Refsum's disease as well as

Address all correspondence to Phyllis Faust, Department of Pathology, Columbia University, PH Stem 15-124, 630 West 168th Street, New York, NY 10032. Tel.: (212) 305-7339. Fax: (212) 305-4548. E-mail: plf3@columbia. edu

1. *Abbreviations used in this paper*: BLBP, brain lipid binding protein; ES, embryonic stem; PBD, peroxisome biogenesis disorder; PC, Purkinje cell; PTS, peroxisomal targeting signal; VLCFA, very long chain fatty acids.

classic rhizomelic chondrodysplasia punctata (RCDP). In these latter disorders, brain malformations are absent or much less prominent than in Zellweger syndrome.

In the Zellweger central nervous system, there is disordered neuronal migration leading to characteristic cytoarchitectonic abnormalities involving the cerebral hemispheres, the cerebellum, and inferior olivary complex (Volpe and Adams, 1972; Evrard et al., 1978). The malformation of the cerebral cortex is most severe and reproducibly results in gyral abnormalities centered around the Sylvian fissure with a stereotypic medial pachygyria and lateral polymicrogyria. These gyral abnormalities reflect a reduced neuronal population in the cortex and large numbers of subcortical heterotopic neurons. These architectonic features, encountered postnatally as well as in pathologic studies on Zellweger fetuses (Powers et al., 1985, 1989), indicate that this malformation results from a developmental disturbance in the migration of neuroblasts to form the cerebral cortical plate throughout much or all of the cytogenetic epoch. In the cerebellum, one finds heterotopic Purkinje cells (PCs) in the white matter, subjacent to intact Purkinje and granule cell laminae, or combinations of abnormally arranged PCs and granule cells (heterotaxias). Dysplastic changes of the principal olivary nucleus and dentate nucleus are seen with a simplification in the normal serpiginous course, laminar discontinuities and condensation of neurons around the periphery of the nuclear islands. In addition, abnormalities develop postnatally in white matter including decreased myelination, reactive astrocytosis, and lipid accumulations in astrocytes.

In the PBDs, there is a block in the posttranslational import of peroxisomal matrix proteins into the organelle, whereas peroxisomal membrane proteins are assembled in the cell into "membrane ghost" structures that appear to be devoid of content (Santos et al., 1987, 1988). The import of matrix proteins bearing the COOH-terminal PTS1 and/or the NH_2-terminal PTS2 peroxisomal topogenic targeting signal (Purdue and Lazarow, 1994; Rachubinski and Subramani, 1995) may be differentially affected in these patients (Motley et al., 1994; Slawecki et al., 1995). Biochemical studies have shown a reduced activity of multiple peroxisomal matrix enzymes in the PBDs. In Zellweger syndrome, the peroxisomal dysfunction is characterized by accumulation of very long chain fatty acids (VLCFA), deficient plasmalogen synthesis, and accumulation of pipecolic acid, phytanic acid, and bile acid intermediates (Lazarow and Moser, 1994).

PBDs are genetically heterogeneous disorders that may arise from defects in at least 11 different genes (Moser et al., 1995). Complementation group 10 (group F in Japan) was the first complementation group for which a genetic defect was defined (Shimozawa et al., 1992) and demonstrated to be a mutation in the peroxisome assembly factor-1 gene (now called *PEX2*; Distel et al., 1996). This zinc-finger–containing, 35-kD peroxisomal integral membrane protein was originally described in a Chinese hamster ovary cell line selected for absence of peroxisomes (Tsukamoto et al., 1990, 1991) and subsequently found to be mutated in another patient with severe Zellweger syndrome (Shimozawa et al., 1993) and two additional Chinese hamster ovary cell lines (Thieringer and Raetz, 1993). The majority of mutations are nonsense mutations leading to premature termination of this protein. The role of Pex2p in peroxisome assembly is not yet understood.

Zellweger syndrome is one of the few human neuronal migration disorders for which genetic defects have been defined. Elucidation of the causal link between absence of peroxisome function and the neuronal migration defect will certainly require the use of animal models, yet no naturally occuring models exist. We have generated a null mutation of the murine *PEX2* gene locus and demonstrated that homozygous *PEX2*-deficient mice show abnormal brain development with a prominent defect in the formation of the cerebral cortex. These mice provide a model system for analyzing the role of peroxisomal function in early phases of development, when cell migration is establishing the form of different brain regions.

Materials and Methods

Cloning of the Mouse PEX2 Gene

A 658-bp fragment of the mouse *PEX2* gene was isolated by PCR using genomic DNA isolated from C57Bl/6 mouse liver and primers based on the rat PEX2 sequence (Tsukamoto et al., 1991). Primers were: forward, 5′-CAGTGCATGAATTTTGTGGTTGGA-3′ extending from position 567; and reverse 5′-CCAGTGATTAGAACTGAGTTGTGC-3′ extending from position 1,225 of the rat mRNA sequence. (PCR cycle parameters are for a thermocycler [480; Perkin Elmer, Norwalk, CT]). After 4 min of denaturation at 94°C and 2 min of renaturation at 60°C, 30 cycles were run with 1.5 min at 72°C, 1 min at 94°C, 1 min at 60°C, followed by a final extension for 10 min at 72°C. A single appropriately sized fragment was obtained, subcloned into pCRII plasmid vector (Invitrogen Corp., San Diego, CA), and sequenced to confirm the identity as a *PEX2* gene (data not shown).

The PCR fragment was used to probe a 129SVJ mouse genomic λFIX II phage library (946309; Stratagene, La Jolla, CA) and a C57BL/6 P6 cerebellum cDNA library in λZAP (kindly provided by G. Dietz, Rockefeller University, New York, NY). These sequence data are available from Genbank/EMBL/DDBJ under accession number AF031128. The deduced genomic structure of the mouse *PEX2* gene is shown in Fig. 1 *A*.

Gene Targeting and Generation of PEX2-deficient Mice

A targeting construct (Fig. 1 *A*) was prepared by ligation of a 5.05-kb BsteII (blunted)–XbaI PEX2 genomic fragment into a pKS-NT vector (Wurst et al., 1994) digested with EcoRI (blunted) and XbaI to yield pNT-BX , followed by ligation of a blunt 2.5-kb HindIII–BstXI PEX2 genomic fragment into the pNT-BX vector digested with SalI (blunted). The targeting vector (50 μg) was linearized with XhoI and electroporated into R1 embryonic stem (ES) cells (5.6×10^6) as previously described (Wurst and Joyner, 1993). Transfected cells were plated onto *neo*^{r}, mitomycin-C–inactivated primary embryonic fibroblasts and double selection (250 μg/ml G418; 0.2 μm gancyclovir) was started 24 h after the electroporation. Resistant ES clones were selected 7 to 9 d after the transfection. Targeted clones were identified by Southern blot hybridization analysis of genomic DNA (Fig. 1 *B*) using probes external to the targeting vector (see below). The frequency of homologous recombination was 10 and 20% of double drug-resistant colonies in two separate electroporations.

Chimeric mice were generated by injection of four ES cell clones into blastocysts of C57BL/6 donor mice as described (Papaioannou and Johnson, 1993). Highly chimeric males from three of the four ES cell lines were intercrossed with C57BL/6 mice, and agouti offspring were tested for germline transmission by Southern blot analysis. Homozygous *PEX2*-deficient mice were obtained by interbreeding F1 heterozygotes; F2 offspring were genotyped by PCR analysis (see below).

Southern Blot Analysis

Genomic DNA of ES cell clones was isolated as described (Wurst and Joyner, 1993) and was restriction digested with EcoRI or BglII for the analysis of homologous recombinants. DNA was transferred to Gene-screen Plus (New England Nuclear, Boston, MA) and hybridized according to

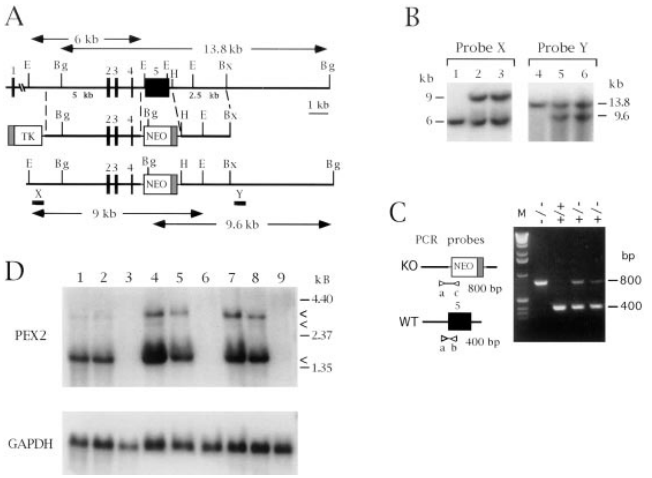

Figure 1. Generation of *PEX2*-deficient mice. (*A*) Schematic representation of the PEX2 genomic locus (*top*), targeting vector (*middle*), and targeted allele (*bottom*). Exon sequences are indicated by the black boxes. Selectable neomycin resistance (*NEO*) and thymidine kinase (*TK*) cassettes, under control of the PGK promoter (*shaded box*), are shown. Dashed lines indicate the region of homology between locus and targeting vector. The origins of the 5′ and 3′ probes (*X* and *Y*) and the size of the resulting restriction fragments (*long arrows*) used to identify the targeted ES cell lines are shown. In the targeted locus, exon 5, containing the translation initiation site and entire coding sequence, is replaced by the NEO gene, resulting in a null allele. *Bg*, BglII; *Bx*, BstXI; *E*, EcoRI; *H*, HindIII; *X*, XbaI. (*B*) Southern blots of genomic DNA isolated from targeted ES cell lines. (Lanes *1–3*) EcoRI digest gives a wild-type 6-kb fragment and targeted 9-kb fragment. (Lanes *4–6*) BglII digest gives a wild-type 13.8-kb fragment and targeted 9.6-kb fragment. (*C*) PCR analysis of tail DNA of wild-type (+/+), heterozygous (+/−), and homozygous (−/−) mice. Primers used for the PCR (*a–c*) are indicated. *M*, BRL 1-kb ladder marker. (*D*) Northern blot hybridization analysis of RNA from liver (lanes *1–3*), brain (lanes *4–6*), and kidney (lanes *7–9*). 20 μg of total RNA from +/+ (lanes *1*, *4*, and *7*), +/− (lanes *2*, *5*, and *8*), and −/− (lanes *3*, *6*, and *9*) newborn mice were hybridized with an exon 5 *PEX2* genomic probe or GAPDH probe. Arrowheads indicate the three *PEX2* transcripts identified. Size marker, BRL RNA ladder.

the manufacturer's protocol. Southern blots were probed with a 0.7-kb BsteII–ClaI PEX2 genomic fragment (5′-probe, probe X) for EcoRI digests or a 0.8-kb BstXI PEX2 genomic fragment (3′-probe, probe Y); both of these probes flank the regions of homology in the targeting vector (Fig. 1 *A*).

PCR Analysis

PCR of genomic tail DNA of wild-type, heterozygous, and homozygous mice was carried out with a set of three primers: primer a (5′-GGGATAGGGTCAAGATA-TAAAGG-3′), primer b (5′-TAGATGGTGAACCTCCACAGGAAA-3′), and primer c (from *neo* gene; 5′-ATGCCTGCTTGCCGAATATCATG-3′). A standard 20-μl reaction contains: ~0.25 μg DNA and 16 pmol of each primer in reaction buffer containing 10 mM Tris-HCl, pH 8.8, 75 mM KCl, and 1.5 mM $MgCl_2$. After denaturation for 3 min at 94°C and renaturation for 2 min at 60°C, 30 cycles were run with 1.5 min at 72°C, 1 min at 94°C, 1 min at 60°C followed by a final extension for 10 min at 72°C. PCR products were analyzed on 2% agarose gels and yielded the wild-type allele of 400 bp and targeted allele of 800 bp (Fig. 1 *C*).

Northern Blot Analysis

Total RNA was isolated by the single-step guanidinium thiocyanate-phenol method (Chomczynski and Sacchi, 1987). RNA (20 μg) from brain, liver, and kidney of newborn mice (P0) was heat denatured and fractionated by electrophoresis through a 1.2% formaldehyde–agarose gel and transferred onto a nylon membrane (Gene-screen; New England Nuclear) by capillary blotting. The filter was hybridized according to the manufacturer's instructions with a randomly ^{32}P-labeled 1.25-kb EcoRI *PEX2* genomic fragment that contains exon 5 (Fig. 1 *A*). The final high stringency wash was done in 0.2× SSC, 1% SDS at 65°C. The filter was then stripped of radioactivity and reprobed with a 1.2-kb PstI fragment of GAPDH DNA.

Biochemical Analyses

VLCFA and Plasmalogens. Blood (~50–100 μl) was collected from newborn mice after decapitation and 10 μl of 7.5% K_3EDTA added to prevent clotting. The sample was centrifuged for 10 min at 1,000 *g* and plasma separated from the pelleted erythrocytes. Samples were stored at −70°C before analysis. Analyses of VLCFA in plasma and erythrocyte plasmalogens were kindly performed for us by Dr. H. Moser and A. Moser (Kennedy Krieger Institute, Baltimore, MD) as described (Bjorkhem et al., 1986; Moser and Moser, 1991).

Liver Fractionation and Catalase Assay. The liver from newborn mice was collected, weighed, and placed in ice-cold 0.25 M sucrose, 1 mM EDTA, 0.1% ethanol, pH 7.4 (SVE) and processed essentially as described (Lazarow et al., 1991). Briefly, each liver was homogenized in 0.75 ml of SVE (10–15 vol) containing 5 μg/ml of leupeptin, pepstatin, and antipain using a motor-driven Potter-Elvehjem homogenizer and a postnuclear supernatant (PNS) prepared. Two thirds of the PNS was centrifuged at 17,000 *g* and separated into supernatant and pellet. Catalase (peroxisomes) and *N*-acetyl-β-glucosaminidase (lysosomes; as an internal control that homogenization was not excessive) were assayed in the postnuclear supernatant, 17,000 *g* supernatant and pellet as previously described (Lazarow et al., 1988). Protein was measured by BCA reagent (Pierce, Rockford, IL).

Immunohistochemistry

Fibroblasts were isolated from skin of newborn mice. The skin was finely minced, digested in trypsin, and plated in DME, 10% heat inactivated fetal calf serum, 100 mM L-glutamine, and 1× antibiotics. Cells were plated on printed microscopic slides (Cel-Line, Newfield, NJ) with 12-mm diam wells that had previously been coated with 0.01 mg/ml poly-L-lysine and fixed 16–20 h after plating with 4% paraformaldehyde for 20 min at room temperature. Antibodies against bovine catalase and rat liver PxIMPs were a gift from P.B. Lazarow (Mount Sinai Hospital, New York, NY); antibody against peroxisomal 3-ketoacyl-CoA thiloase was a gift from T. Hashimoto (Shinshu University School of Medicine, Matsumoto, Nagano, Japan). The procedure for indirect immunofluorescence was essentially as described (Santos et al., 1988) and used 1% NP40 to permeabilize the cells.

Mice at P0 and embryos at E15 were deeply anesthetized and perfused intracardially with 4% paraformaldehyde in PBS, pH 7.4. The brain was removed and postfixed at 4°C for 24 h in the same fixative, rinsed in PBS, and 100-μm sections prepared on a vibratome (coronal plane for forebrain; saggital plane for cerebellum). Sections were permeabilized and blocked in 1% Tween, 20% normal goat serum in PBS for 90 min. Antibodies were diluted in the above buffer and incubated with the sections overnight at 4°C, including: rabbit anti-GFAP (Dako Corporation, Carpinteria, CA) at 1:200, rabbit anti-BLBP (a gift from N. Heintz, Rockefeller University) at 1:1,000, mouse monoclonal antibody RC2 (Misson et al., 1988) at 1:1, and rabbit anti-calbindin D-28k (SWant, Bellinzona, Switzerland) at 1:1,000. Sections were washed three times for 30 min in PBS. Secondary antibody conjugated to fluorescein (Cappel Research Products, Cochranville, PA) was used at 1:200.

Cells and sections were photographed with a microscope (Axiovert; Zeiss, Inc., Thornwood, NY) fitted with fluorescent illumination planneofluor 2.5, 5, 10, 20, 40, and 100× objectives, 1.6× zoom capability, and an Axiophot camera module. For RC2, BLBP, and calbindin D-28k staining, sections were imaged with a confocal scan head (MRC600; Bio Rad, Hercules, CA) and host computer system (PC-AT; IBM, Danbury, CT).

Histology

Brain, spinal cord, and kidney from newborn mice were removed and fixed by immersion in Bouin's fixative for 4 to 20 h at room temperature, followed by rinsing in 70% ethanol. Liver, adrenal, and patella were fixed in 10% formalin. Tissues were embedded in paraffin following standard

procedures, sectioned at 7 to 10 μm, and stained with hematoxylin-eosin. Carefully matched coronal sections of brains were photographed with a microscope (Axiovert; Zeiss, Inc.) and print pictures compared to analyze histologic abnormalities in mutant versus control animals.

Whole mount alizarin red/alcian blue staining of newborn mouse skeletons was performed as previously described (Lufkin et al., 1992).

Electron Microscopy

For morphologic studies, liver and adrenal gland from newborn mice were diced in 2.5% glutaraldehyde in 100 mM cacodylate, pH 7.4, and fixed for 3 to 4 h on ice. The tissues were then postfixed in 1% osmium tetroxide in the same buffer, treated with uranyl acetate, dehydrated in ethanol, propylene oxide, and embedded in Epon.

For DAB catalase cytochemistry, liver pieces were fixed in 2% paraformaldehyde containing 2.5% glutaraldehyde in 100 mM cacodylate, pH 7.4, for 3 h. The alkaline 3,3′-diaminobenzidine (DAB) reaction was carried out as previously described (Shio and Lazarow, 1981). After reaction, the slices were washed, postfixed in osmium tetroxide, and processed as above for morphology.

Grids were viewed in an electron microscope (100 CX; Jeol Ltd., Tokyo, Japan) operated at 80 kV.

Results

Generation of PEX2-deficient Mice

A fragment of the mouse *PEX2* gene was isolated by PCR using genomic mouse liver DNA and primers based on the rat PEX2 sequence (see Materials and Methods). This fragment was used as a probe to isolate genomic and cDNA clones for *PEX2*, and the genomic organization was determined (Fig. 1 *A*). To disrupt the *PEX2* locus, a targeting vector was constructed in which exon 5, containing the translation initiation site and entire coding sequence for the gene, was replaced by the neomycin phosphotransferase gene (Fig. 1 *A*). The targeting construct was electroporated into R1 ES cells (Nagy et al., 1993) and targeted clones identified by Southern blot hybridization (Fig. 1 *B*). Highly chimeric males from three ES cell lines were intercrossed with C57BL/6 mice, and all of them transmitted the mutation through the germline. F1 heterozygous offspring from these three lines were interbred to produce homozygous *PEX2*-deficient offspring. The phenotype of the homozygous *PEX2* mutant mice was the same in all three lines. F2 offspring were genotyped by PCR analysis (Fig. 1 *C*). Northern blot analysis of total RNA of liver, brain, and kidney of newborn mice revealed an absence of *PEX2* transcripts in homozygous mutant mice when an exon 5 genomic fragment was used as a probe (Fig. 1 *D*). Note that in addition to the major mRNA transcript of ~1.8 kb, two other less abundant transcripts are detected (3.9 and 3.25 kb), and all are missing in the homozygous mutant mice. A less abundant transcript of 2.5 kb has been described for human *PEX2* (Shimozawa et al., 1992).

No homozygous mutant mice were found in 175 surviving offspring at 3 to 4 wk of age. A normal Mendelian ratio of wild-type/heterozygous mice was observed at this age (60 +/+:112 +/−), indicating normal survival of heterozygotes. However, among 331 newborn pups (P0), there were 87 wild-type (+/+), 162 heterozygous (+/−), and 82 homozygous (−/−) mice, the ratio being close to 1:2:1. The majority of *PEX2*-deficient mice were observed to die shortly after birth (usually <12 h), do not feed, and display a variable in utero growth retardation (mean 29% weight reduction versus littermate controls, range 12–42%; see Fig. 7 *A*). Although the mutant mice do not feed, one can elicit the normal rhythmic suckling movement of the jaw by mechanical stimulation of the lip (Kutsuwada et al., 1996). Approximately 2% of newborn mutant mice do show small amounts of milk in their stomachs. Rarely, mutant mice have survived up to 1 or 2 d after birth ($n = 3$). There is no obvious facial or limb dysmorphism (see Fig. 7 *A*), and seizures have not been observed. The animals respond normally to noxious stimuli. The *PEX2*-deficient mice move their limbs well but are hypoactive and tend to maintain a "C-shaped," contracted posture. When placed on their paws, the mutants lift their heads poorly and often fall over rapidly. This apparent hypotonia of the mutant mice was evident even in litters of mice obtained very soon after birth and in which none of the animals had fed. In addition, several runted, nonmutant mice have been observed and shown not to display this degree of hypotonia.

Biochemical Abnormalities in PEX2-deficient Mice

Plasma and erythrocyte samples were collected from newborn mice to assay for VLCFA and erythrocyte plasmalogens. Tables I and II show plasma VLCFA and erythrocyte plasmalogen levels, respectively, in control and homozygous-mutant mice along with comparative data from patients with peroxisomal biogenesis disorders. In the *PEX2*-deficient mice there is a marked increase in plasma VLCFA, both saturated and monounsaturated, with an ~8–12-fold increase in the c26/22 ratio and 9.5-fold increase in the c26:0 concentration versus control mice (Table I). These elevations are similar to that seen in human peroxisomal biogenesis disorders. The erythrocyte plasmalogen levels (Table II) are severely deficient in the mutant mice, with a 50–60-fold decrease relative to control mice. This plasmalogen deficiency is most similar to that seen in the disorder RCDP, where the plasmalogen deficiency is most severe. Mice heterozygous for the *PEX2* gene deletion show no significant difference from control mice in plasma VLCFA and erythrocyte plasmalogens.

Absence of functional peroxisomes may also be inferred by the lack of sedimentable catalase in cell homogenates. To directly demonstrate the abnormal cellular localization of catalase, a postnuclear supernatant was prepared from newborn mouse livers and separated into a high speed pellet, containing the cell organelles, and a supernatant. As shown in Table III, catalase was 80% sedimentable in wild-type and heterozygous mice but was 97% soluble in the *PEX2*-deficient mice. The distribution of the lysosomal enzyme marker *N*-acetyl-β-glucosaminidase was not affected by the *PEX2* gene mutation (Table III).

PEX2-deficient Mice Have a Peroxisome Assembly Defect

To determine the cellular localization of peroxisomal matrix and membrane proteins, fibroblast cultures were derived from skin of newborn mice and stained by immunofluorescence using antibodies against catalase, peroxisomal 3-ketoacyl-CoA thiolase, and rat liver peroxisomal integral membrane proteins (PxIMPs). In control fibroblasts, the matrix markers catalase and thiolase show a punctate pattern of immunofluorescence typical of peroxisomes

Table I. Plasma Total Very Long Chain Fatty Acids

Sample	c22%	c24%	c26%	c24/22 Ratio	c26/22 Ratio	c26:0 (μg/ml)	c26:1 (μg/ml)
Mouse							
C57BL/6	0.304	0.340	0.013	1.13	0.05	0.15	0.05
129/white	0.429	0.528	0.025	1.25	0.06	0.30	0.06
109-A5 (+/+)	0.224	0.253	0.023	1.13	0.10	0.21	0.40
109-A4 (−/−)	0.243	0.640	0.201	2.63	0.83	2.05	0.85
4-A3 (−/−)	0.371	0.800	0.276	2.16	0.74	1.95	0.81
4-A4 (−/−)	0.304	0.603	0.226	1.98	0.74	2.05	0.85
Human							
Normal				0.83 (0.01)	0.014 (0.0)	0.33 (0.15)	
Zellweger				2.0 (0.24)	0.49 (0.03)	2.5 (0.85)	
NALD				1.8 (0.35)	0.30 (0.14)	2.4 (0.73)	
Hyperpipecolic acidemia				1.4	0.16	1.7	

Samples from control mice (C57BL/6 and 129) were from adult animals. For the *PEX2* mice, samples are from newborns (P0), and the genotype is shown in parentheses; animals 109-A4, -A5 and 4-A3, -A4 are from two separate litters. For the human data, values shown are the mean and standard deviation (in parentheses; reprinted with permission; Moser and Moser, 1991).
NALD, Neonatal adrenoleukodystrophy.

(Fig. 2, *A* and *C*). Fibroblasts derived from *PEX2*-deficient mice show only diffuse cytoplasmic staining with these antibodies (Fig. 2, *B* and *D*). Thus, both peroxisomal targeting signal (PTS) pathways for import of peroxisomal matrix proteins, as defined here by catalase (PTS1) and thiolase (PTS2), are disrupted in the mutant fibroblasts. Assembly of peroxisomal membrane proteins into "membrane ghosts" (Santos et al., 1988) can be identified in *PEX2*-deficient fibroblasts with the anti-PxIMP antibody (Fig. 2 *F*). As has been described for Zellweger fibroblasts, the membrane ghosts are generally larger in size and fewer in number than normal peroxisomes (compare with Fig. 2 *C*) and are often found in small clusters. Thus, integral membrane proteins of the peroxisome are assembled in fibroblasts of *PEX2*-deficient mice, but matrix proteins are not imported into the organelle.

Table II. Eythrocyte Plasmalogens

Sample	C16 Plasmalogen	C18 Plasmalogen
Mouse		
C57BL/6	0.043	0.053
129	0.049	0.059
101-A3 (+/−)	0.054	0.070
101-A4 (+/+)	0.047	0.058
109-A5 (+/+)	0.061	0.083
109-A4 (−/−)	0.001	0.001
4-A3 (−/−)	0.001	0.001
4-A4 (−/−)	0.001	0.001
Human		
Normal	0.065 (0.010)	0.195 (0.035)
Zellweger	0.008	0.020
NALD	0.01-0.04	0.02-0.01
RCDP	0.001	0.001

The values represent the ratios of C16 or C18 dimethylacetyl derivatives of plasmalogen to the C16 or C18 saturated fatty acids. A low ratio indicates plasmalogen deficiency. Samples from control mice (C57BL/6 and 129) were from adult animals. For the *PEX2* mice, samples are from newborns (P0), and the genotype is shown in parentheses; animals labeled 101-, 109-, and 4- are from three separate litters. For the human data, values shown are the mean and standard deviation (in parentheses; reprinted with permission; Moser and Moser, 1991).
NALD, Neonatal adrenoleukodystrophy.
RCDP, rhizomelic chondrodysplasia punctata.

Morphologic Consequences of a Lack of Peroxisomes

Abnormal Lamination in the Cerebral Cortex. There were no external abnormalities evident in the brain of homozygous *PEX2*-deficient mice at PO; the size and proportion were similar to those of the wild-type and heterozygous mice. Carefully matched coronal sections of the cerebrum were examined by hematoxylin and eosin (H&E) staining and revealed a major abnormality in the developing cerebral cortex of homozygous mutant mice. Low power examination revealed an altered distribution of cells within the developing cortical plate of mutant mice, with a lack of normal layering as well as an increased cellular density in the underlying white matter (intermediate zone) where neurons are still migrating to form the cortex (Fig. 3). The subplate neurons, easily visible in the wild-type brains (Fig. 3, *A* and *C*, *black arrows*), are obscured by the increased density of cells in the lower cortical plate and intermediate zone in mutant mice. These changes are seen over a large expanse of neocortex from medial (Fig. 3 *B*) and lateral (Fig. 3 *D*) regions. In addition, there is a gradient of severity in the morphologic change from medial to lateral cortical regions. In more lateral cortical regions (Fig. 3, *C* and

Table III. Subcellular Distribution of Organelle Enzymes in Liver

		Catalase (peroxisomes)		N-acetyl-β-glucosaminidase (lysosomes)	
Genotype	*n**	Pellet	Supernatant	Pellet	Supernatant
		%			
+/+	4	80	20 (4.3)	88	12 (1.9)
+/−	5	80	20 (3.4)	86	14 (1.6)
−/−	9	3	97 (0.6)	85	15 (2.6)

Results are expressed as the percentage of activity present in pellet plus supernatant. The standard deviation of the data is given in parentheses. Recoveries were 100–111%.
*n**, Number of livers examined.

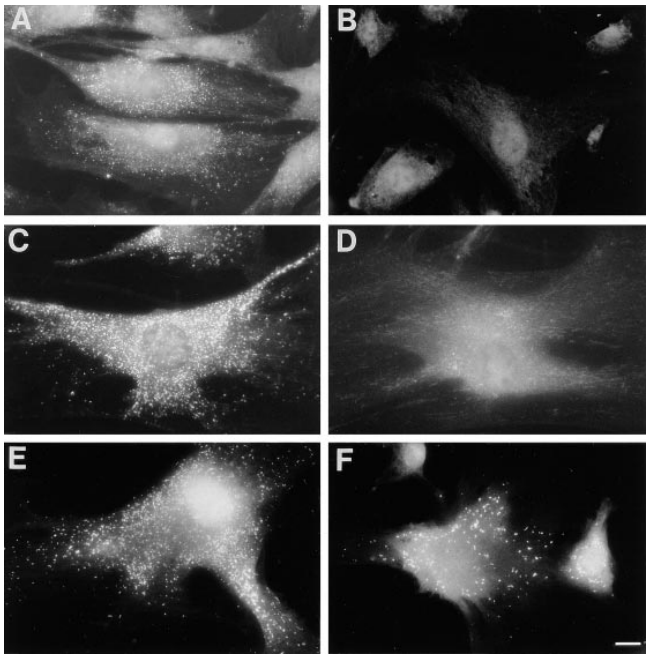

Figure 2. Immunofluorescence staining of wild-type and *PEX2* mutant mouse fibroblasts. Wild-type (*A*, *C*, and *E*) and homozygous mutant (*B*, *D*, and *F*) fibroblasts were stained with antibodies against catalase (*A* and *B*), peroxisomal 3-ketoacyl-CoA thiolase (*C* and *D*), and rat liver peroxisomal integral membrane proteins (*E* and *F*). The mutant fibroblasts assemble peroxisomal membrane proteins into punctate structures in the cell but are unable to import the matrix proteins catalase and thiolase into the peroxisome. Bar, 16 μm.

D), the layer VI/V boundary (indicated by *white arrows*) is easier to discern in the mutant mouse but becomes increasingly blurred as one proceeds medially (third white arrow is absent in Fig. 3 *D*, as boundary is not evident). This boundary is not evident in medial cortical regions (Fig. 3 *B*).

At high power, the abnormal distribution of cells in the cortical plate can be further appreciated (Fig. 4). Note that only layers VI, V, and I (marginal zone) are completely formed in newborn mice and layer IV cells are just arriving in the cortex. In the mutant mice, the marginal zone and subplate are normally formed, and the thickness of the cortical plate is not consistently different from control mice. In medial cortical regions (Fig. 4, *A* and *B*), there is severe effacement of the lamination in the remaining cortical layers seen as a loss of distinction between the layer boundaries (indicated by *white dotted lines* in Fig. 4 *A*) and an altered cell distribution in layers V and VI. This change is most prominent in the region corresponding to layer V; cells that appear to be pyramidal neurons are difficult to identify and are obscured by a large number of cells with rounder, more immature-appearing nuclei, as well as cells with dark-staining, elongated nuclei. These latter cells may represent migrating neuroblasts. In addition, there is a reduction in the amount of neuropil separating cells (normal neuropil shown in *white circle*, Fig. 4 *A*) in the mutants, leading to an apparent alteration in cell packing density. In ventral–lateral cortical regions, the cortex in mutant mice has a more normal lamination with milder abnormalities in cell distribution (Fig. 4, compare *C* and *D*). In this region, it is possible to more clearly visualize the layer boundaries, and the reduction in intervening neuropil is not as severe.

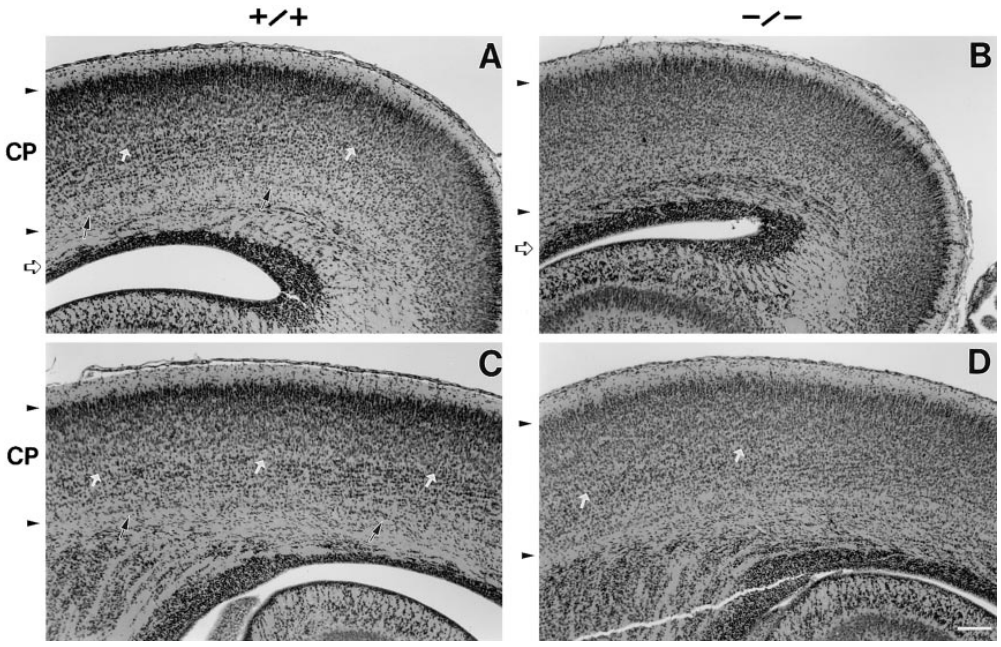

Figure 3. Neuronal migration defect in *PEX2* mutant mice. Matched coronal sections from wild-type (*A* and *C*) and homozygous mutant (*B* and *D*) newborn mouse brains spanning medial (*A* and *B*) and lateral (*C* and *D*) cortical regions, stained with hematoxylin-eosin. The cortical plate (*CP*) is delimited by arrowheads, and the boundary between the germinative zone (*below arrow*) and intermediate zone (*above arrow*) is indicated by an open arrow on the left side (shown in *A* and *B* only). The white arrows indicate the boundary between layers VI and V in the developing neocortex. Note the abnormal layering in the cortical plate of the mutant mouse, with loss of distinction between layer boundaries, and the increased density of cells in the intermediate zone. In more lateral cortical regions (*C* and *D*), the layer VI/V boundary is easier to discern in the mutant mouse but becomes increasingly blurred as one proceeds medially (third white arrow is absent in *D* as boundary is not evident; boundary is not evident in *B*). The subplate (*small black arrows* in *A* and *C*) is obscured in the mutant (*B* and *D*) by the increased density of cells in the lower cortical plate and intermediate zone. Bar, 100 μm.

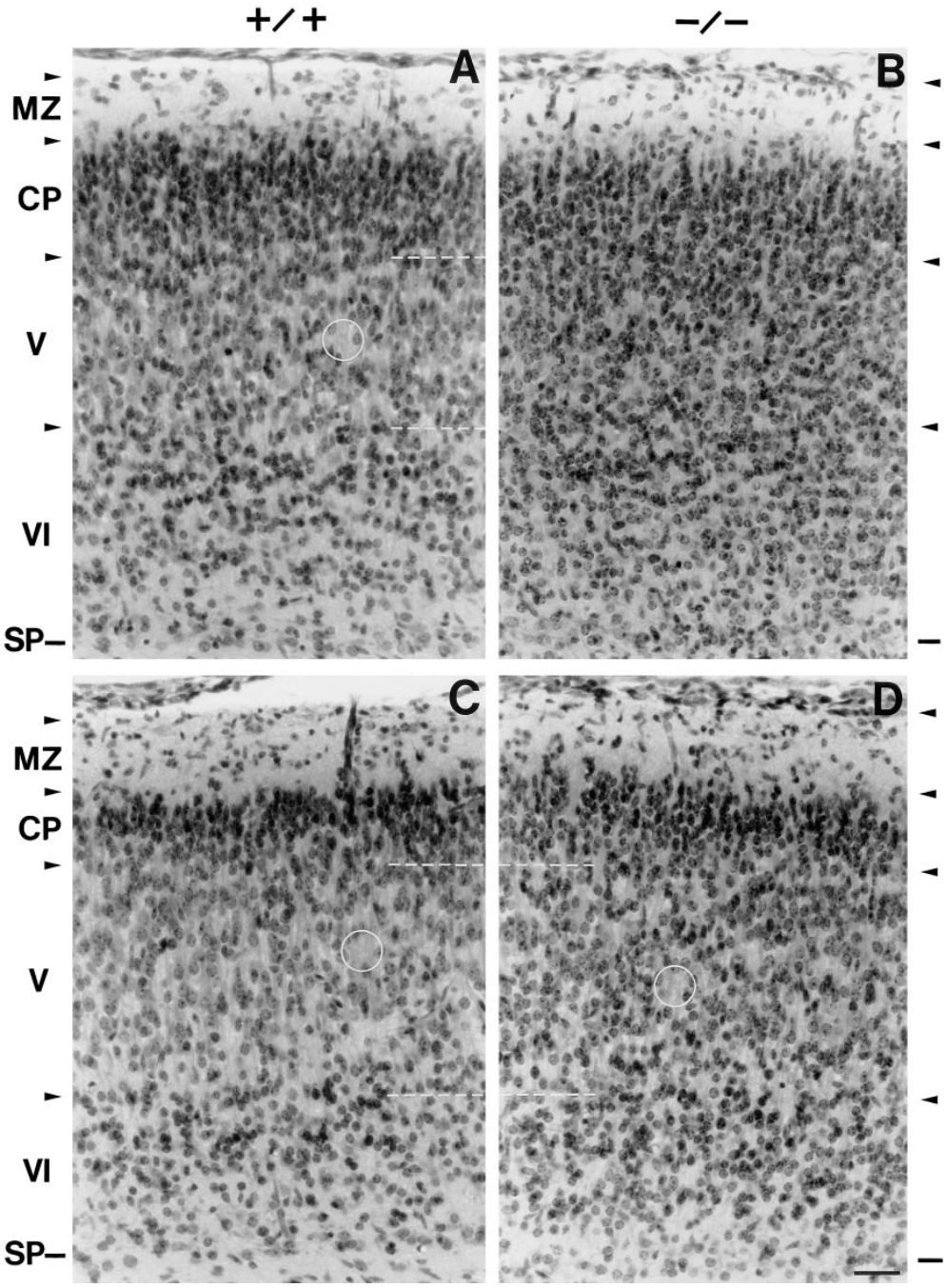

Figure 4. Abnormal cortical lamination. Coronal sections of wild-type (*A* and *C*) and homozygous *PEX2* mutant (*C* and *D*) newborn mouse brains from medial (*A* and *B*) and ventral–lateral (*C* and *D*) cortical regions, stained with hematoxylin-eosin. The cortical layers in the wild-type and "equivalent area" in the mutant are delimited by arrowheads: *MZ*, marginal zone; *CP*, cortical plate; *SP*, subplate. Note the abnormal cortical lamination in the mutant mouse (*B*) with a loss of distinction between the normal layer boundaries (indicated by *white dotted lines* in *A*) and an altered cell distribution, particularly in the layer V region. There is a reduction in intervening neuropil in the mutant (*white circle* in *A* shows normal neuropil). The lamination abnormalities are less severe in the ventral–lateral cortex (*D*). In this region, one can visualize the layer boudaries (*C* and *D*, *white dotted lines*), and the reduction in intervening neuropil is less severe (*white circles*). Bar, 31 μm.

One can still visualize an increased number of cells that appear to be migrating neuroblasts in in the mutant cortex. Rostrocaudal differences in the cortical abnormality were also evident. While the medial cortex was generally abnormal throughout the brain, anterior and posterior cortical regions showed a lesser degree of abnormality throughout a greater extent of lateral cortex (similar to that shown in Fig. 4 *D*; data not shown). Other forebrain regions, including hippocampus, basal ganglia, thalamus, and olfactory bulb, showed no obvious abnormality in the mutant mice. Cortical lamination was normal in heterozygous mice. A total of 16 brains from P0 mutant mice were examined, and all were recognizably abnormal to blinded observers.

There was significant variation in the cortical malformation between mutant mice with different parents. In some animals the defect was much less severe (similar to that in lateral cortex, Fig. 4 *D*), with fewer cells in the underlying white matter and a more limited rostrocaudal extent, being apparent only in central regions of the brain (data not shown). The presence of the cortical malformation and variation within was not attributable to the size of the animal since (*a*) mutant mice of similar size showed significant differences, and (*b*) control, runted animals did not show similar cortical changes (data not shown).

To examine the radial glial scaffold, which serves as the guidance substrate for cortical neuronal migration, brains from E15 mice were stained with antibodies against RC2 and brain lipid binding protein (BLBP), both markers for

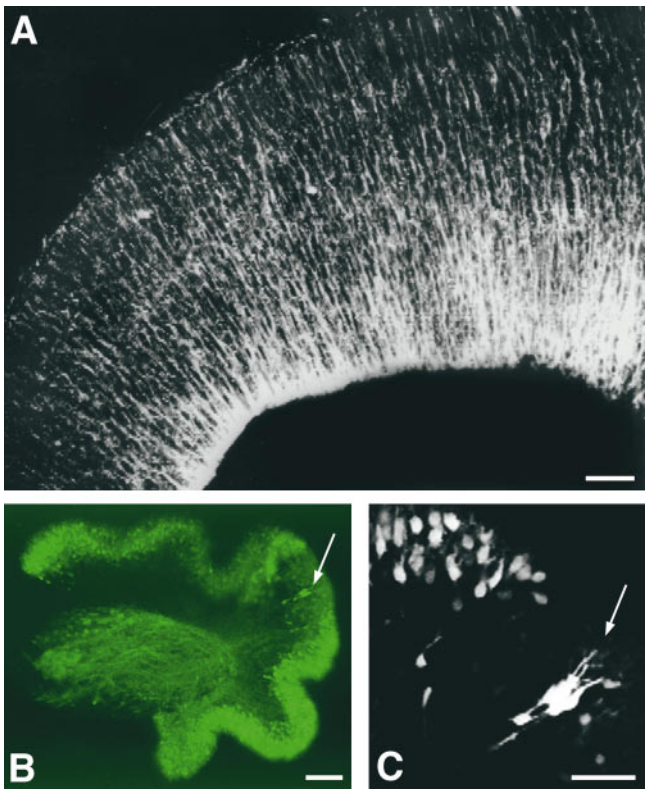

Figure 5. Immunofluorescence staining of forebrain and cerebellum. (*A*) Coronal section of E15 forebrain from *PEX2* mutant mouse stained with RC2 antibody to label the radial glia. (*B* and *C*) Saggital section of P0 cerebellum from *PEX2* mutant mouse stained with calbindin-D28k antibody to label the Purkinje cells (PCs). Anterior is to the left. Arrow indicates small cluster of bipolar PCs slightly beneath the multilayer, shown at higher power in *C*, indicating a slight delay in the migration of these PCs. Images in *A* and *C* were obtained by confocal microscopy. Bars: (*A* and *C*) 50 μm; (*B*) 100 μm.

radial glia (Misson et al., 1988; Feng et al., 1994). RC2 and BLBP immunostains showed no obvious abnormality in the radial glial scaffold in brains from homozygous *PEX2*-deficient mice (Fig. 5 *A*; BLBP not shown).

Brains of P0 mutant mice stained with antibodies against the astrocyte marker GFAP and neuronal marker MAP2 revealed a normal distribution of labeled cells (data not shown).

Inferior Olivary Nucleus, Cerebellum and Spinal Cord

Coronal sections of the hindbrain of P0 mice were examined by serial sections throughout the rostrocaudal extent of the inferior olivary nucleus. In rodents, the principal olivary nucleus is a simple u-shaped structure that lacks the convolutions seen in humans. In the homozygous mutant mice, the component olivary nuclei were normal in position, and there was no evidence of discontinuities in the principal olivary nucleus (data not shown). Preliminary histologic analysis of the principal olivary nucleus in the homozygous *PEX2* mutant mice suggests that there may be subtle abnormalities in the shape as well as neuropil of this nucleus; however, these findings remain to be substantiated.

Histologic sections of the cerebellum in P0 mutant mice revealed that the deep cerebellar nuclei and the external granular cell layer were normally formed and folial development was appropriate for the age of the animal. Examination of the P0 cerebellum with antibodies against calbindin-D28k, a PC marker, demonstrated that the vast majority of PCs in mutant mice had reached a normal position within a multilayer beneath the cerebellar surface (Fig. 5 *B*). These cells had a normal morphology for an early postmigratory PC with numerous thin perisomatic processes (Baptista et al., 1994). In one of three mutant mice examined, a small cluster of PCs was seen slightly beneath the PC multilayer (Fig. 5 *B*, *arrow*). These cells had a bipolar morphology with a few long processes, consistent with an earlier embryonic migratory phase (Fig. 5 *C*), indicating a slight delay in the migration and differentiation of these few cells relative to the majority of PCs. Similar cells were not identified in wild-type mice at P0. Due to the early death of the mutant animals and the immature status of the mouse cerebellum at birth, it is not possible to exclude abnormal positioning of PCs and/or granule cells once the internal granule cell layer has formed (complete by ~P14).

The absence of major morphologic changes in the inferior olive or cerebellum is not due to regional differences in expression of the *PEX2* gene product. RNA in situ hybridization studies showed a diffuse distribution of the *PEX2* transcript in normal mouse brain (data not shown).

Histologic sections of the spinal cord in P0 mutant mice were examined from cervical, thoracic, lumbar, and sacral regions and revealed no obvious abnormality. Lipidosis of neurons, as described by Powers et al. (1987) in Zellweger patients, was not seen.

Liver, Adrenal Gland, Kidney, and Eye

The liver of newborn mutant mice was normal in size and showed no light microscopic abnormalities (data not shown). In electron microscopic analysis of control livers, peroxisomes stain with the cytochemical procedure for catalase (Fig. 6 *A*) and appear as small round or oval forms with an electron-dense urate oxidase core (6 *A*, *inset*), characteristic of rodent peroxisomes. Catalase-reactive particles were not identified in livers from *PEX2*-deficient mice, and there was no obvious morphologic abnormality in the mitochondria (Fig. 6 *B*), which reportedly show distortion in shape and matrix condensation in some Zellweger patients (Goldfischer et al., 1973). Immunofluorescence staining of frozen livers from newborn mice with antibodies against catalase also showed diffuse cytoplasmic staining in all of the hepatocytes in the mutant mice, consistent with the cytosolic localization of catalase (data not shown).

Light microscopic examination of the adrenal gland in newborn *PEX2*-deficient mice revealed adrenocortical cells containing clear clefts (Fig. 6 *C*). These inclusions tended to be located in adrenocortical cells within deeper regions of the adrenal cortex. Similar structures were not observed in wild-type or heterozygote littermate controls. Electron microscopic examination confirmed the presence of gently curved to curvilinear clefts associated with electron dense leaflets (Fig. 6, *D–F*). The clefts ranged in size from 40 to 435 nm. These structures are consistent with the lamellar lipid profiles seen in the adrenal cortex of Zellweger and adrenoleukodystrophy patients (Powers and Schaumberg,

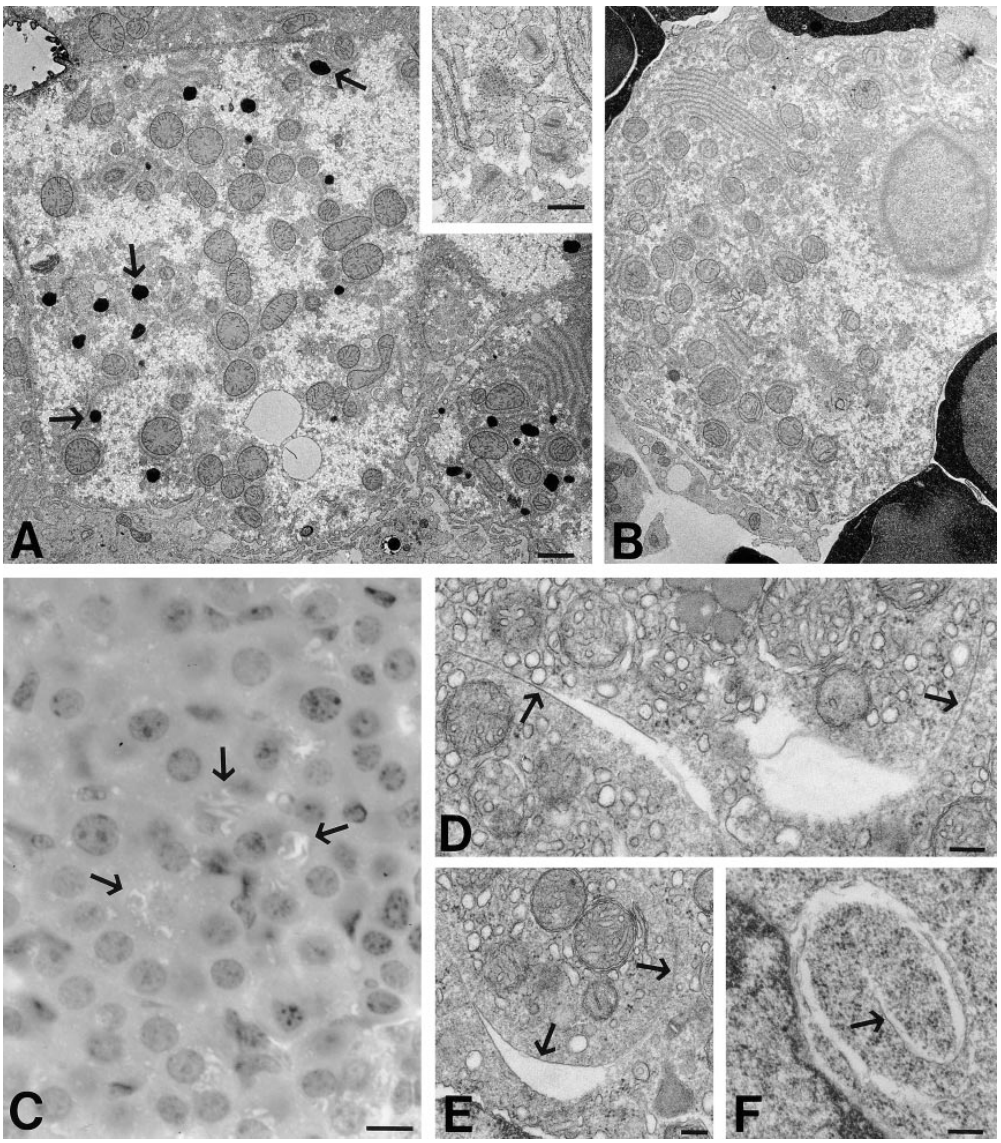

Figure 6. Morphologic changes in liver and adrenal gland. (*A* and *B*) Diaminobenzidine-catalase cytochemistry of wild-type (*A*) and *PEX2* mutant (*B*) liver. Numerous dark staining peroxisomes are only identified in the wild-type liver (*arrows*). Inset in *A* shows characteristic morphology of rodent peroxisomes with a curvilinear, electron-dense core. (*C*) Light microscopic examination of adrenal gland from *PEX2* mutant mouse showing numerous clear clefts (*arrows*) consistent with lipid inclusions. Hematoxylin-eosin stain. (*D–F*) Electron microscopic examination of adrenal gland from *PEX2* mutant mouse showing characteristic lamellar-lipid profiles. Arrows in *D* through *F* indicate lamellae. Cells in *D* and *E* are adrenocortical cells. Cell in *F* is a mesenchymal cell or an adrenocortical precursor. Bars: (*A* and *B*) 100 μm; (*inset*) 400 μm; (*C*) 10 μm; (*D–F*) 200 nm.

1973; Goldfischer et al., 1983). Complex, multilamellate inclusions were not identified.

Light microscopic analysis of the kidneys from newborn mice showed only a slight tubular ectasia in PEX2-deficient mice versus littermate controls (data not shown). There was no evidence of tubular or glomerular cysts in mutant mice. Light microscopic examination of the eyes of newborn mutant mice showed no obvious abnormality (data not shown).

Skeleton

In the Zellweger syndrome, there are characteristic dysmorphic facial features that occur in essentially all patients and stippled calcifications of patellae, femora, and humeri (occur in ~69% of patients; Moser et al., 1995). Characteristic facial features include high forehead, hypertelorism, epicanthal folds, hypoplastic supraorbital ridge, and depressed bridge of nose. Many patients also have wide cranial sutures and large fontanelles. In the newborn *PEX2*-deficient mice, there is no obvious external facial dysmorphism (Fig. 7 *A*). Examination of the entire mouse skeleton by alcian blue (cartilage) and alizarin red (bone) staining and by radiographic examination showed a normal axial and extremity skeleton and no evidence of calcific stippling in the patella or epiphyses of long bones (data not shown). The bones of the calvarium in the homozygous mutant mice did show a delay in membranous ossification characterized by (*a*) a reduced amount of bone with a mottled appearance in the medial frontal bones and the interparietal bone (Fig. 7, *E–H*), and (*b*) an expanded, oval shape at the medial apposition of the frontal bones (analogous to the anterior fontanelle region in humans) and enlargement of the "posterior fontanelle region" formed by the juncture of the parietal and interparietal bones (see especially Fig. 7, *G* and *H*). The majority (70%) of calvaria in control animals are more extensively mineralized and have closely opposed frontal bones (Fig. 7 *B*). In 19% of control mice, there was a slight opening between the medial frontal bones (Fig. 7 *C*) but no significant reduction in bone density. However, the calvarial phenotype of the mutant mice correlated with the size of the animal rather than the geno-

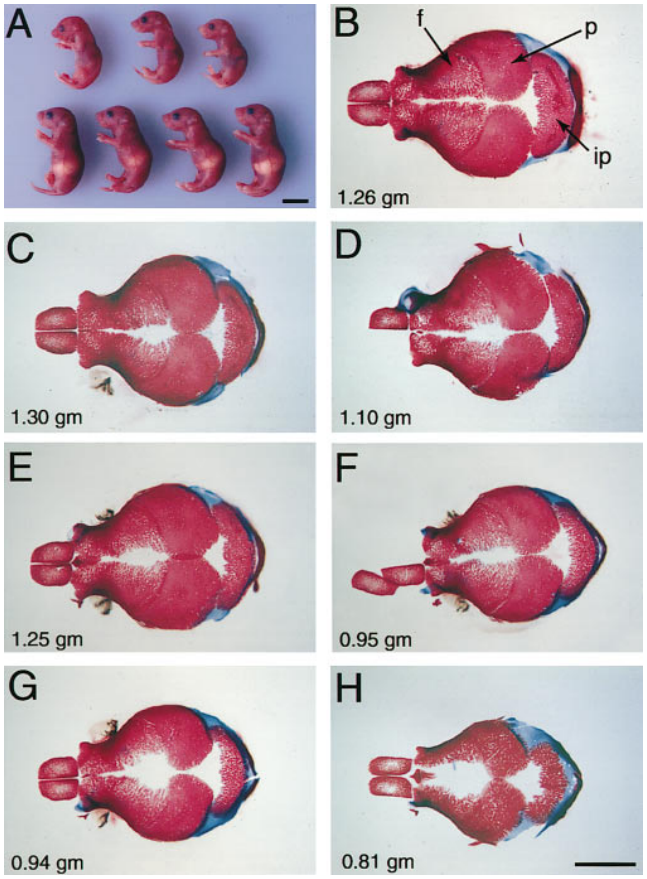

Figure 7. External appearance and cranial morphology of *PEX2* mutant mice. (*A*) Litter of newborn mice with three mutant animals (*top row*) and four control animals (*bottom row*). Note the absence of milk in the stomach and variable size in the mutant animals. Abnormal facies are not evident in the mutant mice. (*B–H*) Alcian blue (cartilage) and alizarin red (bone) staining of newborn mouse calvarium. The weight of each mouse is shown. (*B*) Typical appearance of the calvarium in control animals (70%). *f*, Frontal bone; *p*, parietal bone; *ip*, interparietal bone. (*C*) Control animal with slightly open "anterior fontanelle" but relatively normal bone density (19%). (*D*) Runted, control animal showing slight enlargement of fontanelle space and reduced bone density in medial frontal and interparietal bone. (*E–H*) Homozygous mutant mice, demonstrating the correlation of increasing severity in reduction of bone density in frontal and interparietal bones and enlargement of fontanelle spaces with decreasing size of the animal. Bars, 1 cm.

type, as (*a*) runted wild-type or heterozygous animals showed a similar defect (11% of control animals; weight <1.12 gm; Fig. 7, compare *D* and *F*), and (*b*) larger mutant mice showed a lesser degree of abnormality (Fig. 7, *E* and *F*). The remaining facial bones and base of skull bones were normal in appearance and proportionate in size in the mutant mice.

Discussion

Zellweger syndrome is a unique peroxisomal disorder that results in characteristic central nervous system malformations. We have demonstrated that mice with a complete absence of the *PEX2* gene product have a peroxisomal biogenesis disorder with deficiencies in peroxisomal biochemical functions and morphologic changes in a number of organ systems, including the presence of a prominent defect in the development of the cerebral cortex. These findings confirm the genetic linkage of the *PEX2* defect in humans and the prime importance of absent peroxisomal function in causing the multiple anomalies associated with the Zellweger syndrome.

In Zellweger syndrome, multiple peroxisomal matrix enzymes are deficient due to abnormal assembly of the peroxisomal organelle. Homozygous *PEX2*-deficient mice have a marked increase in plasma VLCFA and deficient synthesis of plasmalogens in erythrocytes. Fractionation of liver demonstrated that the matrix enzyme catalase was present in the cytosol in mutant mice rather than in its normal particulate location. Morphologic studies on fibroblasts and liver from mutant animals confirmed the absence of normal peroxisomes in these tissues. Hepatocytes in the mutant mice did not contain any normal peroxisomes, indicating absence of mosaicism in the liver, as has been reported in some Zellweger patients as well as in the recently described peroxisomal fatty acyl-coenzyme A oxidase-deficient mice (Fan et al., 1996). In fibroblasts, both the PTS-1 and -2 targeting pathways for import of peroxisomal matrix proteins were disrupted in mutant animals, and peroxisomal membrane proteins were assembled into structures consistent with the "membrane ghosts" described in Zellweger patients (Santos et al., 1988). Motley et al. (1994) and Slawecki et al. (1995) have described heterogeneity in the disruption of the PTS-1 and -2 import pathways amongst fibroblasts from PBD patients in different complementation groups, such that one or both pathways are disrupted. Patients with a *PEX2* defect (complementation group 10) were found to have complete disruption of both pathways (Slawecki et al., 1995), as also seen in *PEX2* mutant mice.

The central nervous system malformations are the most consistent feature of the Zellweger syndrome with the characteristic array of cerebral cortical, inferior olivary, and cerebellar changes. In *PEX2*-deficient mice, there is disordered lamination of the cerebral cortex and an increased cell density in the underlying white matter, indicating an abnormality of neuronal migration. Similar to the human condition, the cortex was not uniformly affected; both medial–lateral and anterior–posterior gradients in severity were observed in the mutant mice brains. While the less severe involvement of the ventral–lateral cortex might reflect the greater degree of maturation normally found in the earlier-formed lateral neocortex, the observed anterior–posterior changes do not follow the normal anterior to posterior gradient of cortical maturation (Bayer and Altman, 1991), suggesting an independent mechanism. In the human Zellweger brain, the cortical plate is significantly thinner than in normal brains. However, this was not consistently observed in the *PEX2*-deficient mice, suggesting that the malformation is less severe in the mouse than in humans. This may reflect (*a*) the much smaller size of the mouse neocortex, which contains ~1,000-fold fewer neurons than the human neocortex (Rakic, 1995), and consequently the much smaller distance that migrating neurons must traverse to reach the cortical plate; (*b*) a major difference in the duration of the migratory epoch in hu-

mans (months) as opposed to mice (days), with cumulative damage accruing over time; and (*c*) differences in genetic background, with other as yet undefined genes affecting the phenotypic expression of the peroxisomal defect. Immunohistochemical examination of the radial glial scaffold, which serves as the guidance substrate for cortical neuronal migration, did not reveal any obvious structural abnormalities in the mutant mice. However, this does not exclude the presence of ultrastructural or functional abnormalities in the radial glial cells induced by the lack of peroxisomal function.

The inferior olive and cerebellum also show characteristic changes in the Zellweger syndrome. In the PEX2-deficient mice, major morphologic changes were not observed in the inferior olive or dentate nucleus. These nuclei are much simpler, nonlaminated structures in the rodent, reflecting the much smaller size of the lateral cerebellar cortex in rodents versus humans (Altman and Bayer, 1997). Preliminary histologic analysis of the principal olivary nucleus in the *PEX2* mutant mice suggests that there may be subtle abnormalities in the shape as well as neuropil of this nucleus; however, these findings remain to be substantiated with more detailed studies of olivary morphology and olivocerebellar connectivity. In the cerebellum of mutant mice, subcortical PC heterotopias were not detected. Although the vast majority of PCs reached the multilayer beneath the cerebellar surface, a small cluster of PCs with a slight delay in migration was detected in one mutant mouse. Thus there may be limited and subtle abnormalities in PC migration in the *PEX2*-deficient mice. Due to the early death of the mutant animals and the immature status of the mouse cerebellum at birth, it is not possible to evaluate many aspects of cerebellar development. Therefore, we cannot exclude that during the inward migration of external granule cells from the surface of the cerebellum to form the internal granule cell layer that PC heterotopias might result subjacent to the internal granule cell layer as well as the abnormal arrangements of granule cells and PCs that characterize heterotaxias seen in the Zellweger syndrome. In the neurologic mutant mouse *reeler*, there are extensive subcortical PC heterotopias (more severe than seen in Zellweger syndrome) and shape changes in the principal olivary nucleus (Goffinet et al., 1984), suggesting a relationship between the migratory abnormalities in these cell populations, as has also been suggested in Zellweger syndrome (Evrard et al., 1978). As olivocerebellar topography is established as early as E15 in the mouse (Paradies and Eisenman, 1993), the absence of major olivary changes or subcortical PC heterotopias suggests that malformations that might occur in the *PEX2*-deficient mice, were they to survive longer, are likely to be mild.

Light and electron microscopy analysis of the adrenal gland in mutant mice demonstrated structures consistent with the lamellar–lipid inclusions described in Zellweger syndrome (Goldfischer et al., 1983). The chemical composition of these inclusions is unknown. They are postulated to be phospholipids containing saturated VLCFA.

Some morphologic features of the Zellweger syndrome were not modeled by the *PEX2*-deficient mice. As structural changes in the liver, eye, and brain white matter occur during the postnatal period in Zellweger syndrome, one would not expect to see changes in a newborn animal. Renal cysts, seen in ~93% of Zellweger patients (Moser et al., 1995) and evident in the fetal period (Powers et al., 1985), were not found in kidneys of newborn mutant mice. The slight tubular ectasia seen in the *PEX2* mutant mouse kidneys may reflect early damage and a precursor lesion. Stippled joint calcifications, seen in ~69% of Zellweger patients, were also not identified in *PEX2*-deficient mice. The facial dysmorphism of this syndrome is a central diagnostic feature. However, abnormal facies were not evident in the mutant mice. Zellweger patients are also reported to have enlarged cranial fontanelles. Examination of the mouse skeleton initially suggested the presence of delayed cranial bone mineralization and a larger fontanelle space in the mutant mice. However, this was found to correlate with growth retardation of the animal rather than the mutant genotype. It remains possible that the enlarged fontanelles found in Zellweger patients are also an effect of growth retardation.

The exact cause of death in the *PEX2*-deficient animals has not been established. Shortly after birth, the mutant mice are normal in color and respiratory pattern, and the heart and lungs are normal in size, suggesting absence of a primary respiratory or circulatory defect. While the inability of the mice to feed certainly contributes to their early demise, the mutant animals die sooner than control animals that have not fed. This suggests toxic accumulation of a metabolic product(s) due to the lack of peroxisomal function, which may be exacerbated by dehydration in these animals.

Establishment of normal cerebral cortical lamination involves several defined steps, including proliferation and early specification of neurons within the ventricular zone, attachment to and migration along radial glial guides, followed by detachment from radial glia and assembly into cortical layers. Examination of migrating neurons, both in vivo (Rakic, 1972) and in vitro (Gregory et al., 1988; Hatten, 1990; Rivas and Hatten, 1995), reveals a characteristic morphology with a thick leading process that wraps around the radial glial fiber, a posterior positioning of the nucleus, and a thin trailing process. Neuronal–glial interactions mediated by the molecule astrotactin (Fishell and Hatten, 1991; Zheng et al., 1996), as well as cell–matrix adhesions (Jessell, 1988; Fishman and Hatten, 1993; Sheppard et al., 1995) and cytoskeletal elements (Rivas and Hatten, 1995), are all believed to be important in the migratory process. It remains to be established how the absence of peroxisomal function in Zellweger syndrome may disrupt any or all of these processes. It has been postulated that elevations of VLCFA and bile acid intermediates may play a toxic role in the Zellweger neuronal migration defect (Powers et al., 1989; Kaufmann et al., 1996). Accumulations of lipid products in migrating neurons and radial glia have been documented in Zellweger fetuses (Powers et al., 1989). In addition, specific cellular processes may be disrupted. Recently, mutations in homologues for the *PEX2* gene (Berteaux-Lecellier at al., 1995) and the *LIS-1* gene (Xiang et al., 1995), which is abnormal in the Miller-Dieker lissencephaly syndrome (Reiner et al., 1993; Hattori et al., 1994), have been identified in filamentous fungi, and both cause abnormalities in processes involving nuclear migrations within the cell. While Miller-Dieker lissencephaly has a more severe neuronal migration defect than seen in Zellweger

syndrome, it shares a common spectrum of affected brain regions, including cerebral cortical gyral abnormalities (pachygyria or agyria), inferior olive dysplasia and heterotopias, and PC heterotopias (Norman et al., 1995). Thus, these diverse gene mutations may affect cellular mechanisms common to nuclear migrations and the translocation of the neuronal cell soma along the radial glial fiber.

The *PEX2*-deficient mice provide an important animal model for Zellweger syndrome and a major step toward deciphering the cellular mechanisms of this neuronal migration disorder. Zellweger syndrome displays abnormalities in cortical foliation pattern (pachgyria, polymicrogyria) as well as heterotopias that are commonly seen in many human neuronal migration disorders. As cell migration and the formation of neuronal layers occurs prenatally in the mouse, this system can be used to study the role of peroxisomes in these key steps of brain development. Despite the many differences between human and mouse brain development, the presence of a cortical defect in the *PEX2*-deficient mice indicates a conservation in the mechanisms for neuronal migration. Thus, this mouse model can serve as a system to elucidate the role of peroxisomal function in neuronal migration as well as to unveil general mechanisms for cortical neuronal migration and the establishment of lamination.

We would like to thank Dr. H. Moser and A. Moser for performing the VLCFA and plasmalogen analyses; J.M. Powers for electron microscopy on the adrenal glands and help with the histologic analysis; A. Nagy for providing the R1 ES cells; K. Millen for assistance in making the chimeric mice; H. Shio for technical assistance with the electron microscope; and F. Vito and R. Alcarez for technical assistance with paraffin sections.

This work was supported by National Institutes of Health grants NS-15429 (M.E. Hatten) and the Howard Hughes Medical Institute Physician Postdoctoral Fellowship Program (P.L. Faust).

Note Added in Proof. While this manuscript was in review, Baes et al. published another mouse model for Zellweger syndrome by targeted deletion of the *Pxr1* gene (*PEX5*) that encodes the PTS-1 receptor (*Nat. Genet.* 1997. 17:49–57). The phenotype of the *Pxr1* −/− mouse is very similar to the *PEX2* −/− mouse.

Received for publication 28 July 1997 and in revised form 16 September 1997.

References

Altman, J., and S.A. Bayer. 1997. Comparative anatomy of the cerebellum: an evolutionary perspective. *In* Development of The Cerebellar System. CRC Press Inc., New York. 2–25.

Baptista, C.A., M.E. Hatten, R. Blazeski, and C.A. Mason. 1994. Cell-cell interactions influence survival and differentiation of purified purkinje cells in vitro. *Neuron.* 12:243–260.

Bayer, S.A., and J. Altman. 1991. Overview of global neurogenetic gradients in the neocortex and limbic cortex. *In* Neocortical Development. Raven Press, New York. 30–45.

Berteaux-Lecellier, V., M. Picard, C. Thompson-Coffe, D. Zickler, A. Panvier-Adoutte, and J.-M. Simonet. 1995. A nonmammalian homolog of the PAF1 gene (Zellweger syndrome) discovered as a gene involved in caryogamy in the fungus *Podospora anserina. Cell.* 81:1043–1051.

Bjorkhem, I., L. Sisfontes, B. Bostrom, B.F. Kase, and R. Blomstrand. 1986. Simple diagnosis of the Zellweger syndrome by gas-liquid chromatography of dimethylacetals. *J. Lipid Res.* 27:786–791.

Chomczynski, P., and N. Sacchi. 1987. Single-step method of RNA isolation by acid guanidinium thiocyanate-phenol-chloroform extraction. *Anal. Biochem.* 162:156–159.

Distel, B., R. Erdmann, S.J. Gould, G. Blobel, D.I. Crane, J.M. Cregg, G. Dodt, Y. Fujiki, J.M. Goodman, W.W. Just, et al. 1996. A unified nomenclature for peroxisome biogenesis factors. *J. Cell Biol.* 135:1–3.

Dobyns, W.B., and C.L. Truwit. 1995. Lissencephaly and other malformations of cortical development: 1995 update. *Neuropediatrics.* 26:132–147.

Evrard, P., V.S. Caviness, Jr., J. Prats-Vinas, and G. Lyon. 1978. The mechansim of arrest of neuronal migration in the Zellweger malformation: an hypothesis based on cytoarchitectonic analysis. *Acta Neuropathol. (Berl.).* 41: 109–117.

Fan, C.-Y., J. Pan, R. Chu, D. Lee, K.D. Kluckman, N. Usuda, I. Singh, A.V. Yeldandi, M.S. Rao, N. Maeda, et al. 1996. Hepatocellular and hepatic peroxisomal alterations in mice with a disrupted peroxisomal fatty acyl-coenzyme A oxidase gene. *J. Biol. Chem.* 271:24698–24710.

Feng, L., M.E. Hatten, and N. Heintz. 1994. Brain lipid-binding protein (BLBP): a novel signaling system in the developing mammalian CNS. *Neuron.* 12:895–908.

Fishell, G., and M.E. Hatten. 1991. Astrotactin provides a receptor system for CNS neuronal migration. *Development.* 113:755–756.

Fishman, R.B., and M.E. Hatten. 1993. Multiple receptor systems promote CNS neural migration. *J. Neurosci.* 13:3485–3495.

Goffinet, A.M., K.-F. So, M. Yamamoto, M. Edwards, and V.S. Caviness, Jr. 1984. Architectonic and hodological organization of the cerebellum in reeler mutant mice. *Dev. Brain Res.* 16:263–276.

Goldfischer, S., C.L. Moore, A.B. Johnson, A.J. Spiro, M.P. Valsamis, H.K. Wisniewski, R.H. Ritch, W.T. Norton, I. Rapin, and L.M. Gartner. 1973. Peroxisomal and mitochondrial defects in the cerebro-hepato-renal syndrome. *Science.* 182:62–64.

Goldfischer, S., J.M. Powers, A.B. Johnson, S. Axe, F.R. Brown, and H.W. Moser. 1983. Striated adrenocortical cells in cerebro-hepato-renal (Zellweger) syndrome. *Virchows Arch. A Pathol. Anat. Histopathol.* 401:355–361.

Gregory, W.A., J.C. Edmondson, M.E. Hatten, and C.A. Mason. 1988. Cytology and neuron-glial apposition of migrating cerebellar granule cells *in vitro. J. Neurosci.* 8:1728–1738.

Hatten, M.E. 1990. Riding the glial monorail: a common mechanism for glial-guided neuronal migration in different regions of the developing mammalian brain. *Trends Neurosci.* 13:179–184.

Hattori, M., H. Adachi, M. Tsujimoto, H. Arai, and K. Inoue. 1994. Miller-Dieker lissencephaly gene encodes a subunit of brain platelet-activating factor acetyl-hydrolase. *Nature.* 370:216–218.

Jessell, T.M. 1988. Adhesion molecules and the hierarchy of neural development. *Neuron.* 1:3–13.

Kaufmann, W.E., C. Theda, S. Naidu, P.A. Watkins, A.B. Moser, and H.W. Moser. 1996. Neuronal migration abnormality in peroxisomal bifunctional enzyme defect. *Ann. Neurol.* 39:268–271.

Kutsuwada, T., S. Kenji, T. Manabe, C. Takayama, N. Katakura, E. Kushiya, R. Natsume, M. Watanabe, Y. Inoue, T. Yagi, et al. 1996. Impairment of suckling response, trigeminal neuronal pattern formation, and hippocampal LTD in NMDA receptor e2 subunit mutant mice. *Neuron.* 16:333–344.

Lazarow, P.B., and H.W. Moser,. 1994. Disorders of peroxisome biogenesis. *In* The Metabolic and Molecular Basis of Inherited Disease. C.R. Scriver, A.L. Beaudet, W.S. Sly, and D. Valle, editors. McGraw Hill, New York. 2287–2324.

Lazarow, P.B., G.M. Small, M. Santos, H. Shio, A. Moser, H. Moser, A. Esterman, V. Black, and J. Dancis. 1988. Zellweger syndrome amniocytes: morphological appearance and a simple sedimentation method for prenatal diagnosis. *Pediatr. Res.* 24:63–67.

Lazarow, P.B., R. Thieringer, G. Cohen, T. Imanaka, and G. Small. 1991. Protein import into peroxisomes in vitro. *In* Methods in Cell Biology, Vol. 34. A.M. Tartakoff, editor. Academic Press, San Diego. 303–326.

Lufkin, T., M. Mark, C.P. Hart, P. Dolle, M. LeMeur, and P. Chambon. 1992. Homeotic transformation of the occipital bones of the skull by ectopic expression of a homeobox gene. *Nature.* 359:835–841.

Misson, J.P., M.A. Edwards, M. Yammamoto, and V.V. Caviness, Jr. 1988. Identification of radial glial cells within the developing murine central nervous system: studies based upon a new immunohistochemical marker. *Dev. Brain Res.* 44:95–108.

Moser, H.W., and A.B. Moser. 1991. Measurements of saturated very long chain fatty acids in plasma. *In* Techniques in Diagnostic Human Biochemical Genetics. F.E. Hommes, editor. Wiley-Liss, New York. 177–191.

Moser, A.B., M. Rasmussen, S. Naidu, P.A. Watkins, M. McGuiness, A.K. Hajra, G. Chen, G. Raymond, A. Liu, D. Gordon, et al. 1995. Phenotype of patients with peroxisomal disorders subdivided into sixteen complementation groups. *J. Pediatr.* 127:13–22.

Motley, A., E. Hettema, B. Distel, and H. Tabak. 1994. Differential protein import deficiencies in human peroxisome assembly disorders. *J. Cell Biol.* 125: 755–767.

Nagy, A., J. Rossant, R. Nagy, W. Abramow-Newerly, and J. Roder. 1993. Derivation of completely cell culture-derived mice from early passage embryonic stem cells. *Proc. Natl. Acad. Sci. USA.* 90:8424–8428.

Norman, M.G., B.C. McGillivray, D.K. Kalousek, A. Hill, and K.J. Poskitt. 1995. Neuronal migration disorders and cortical dysplasias. I. Migration disorders. *In* Congenital Malformations of the Brain: Pathologic, Embryologic, Clinical, Radiologic and Genetic Aspects. Oxford University Press, New York. 223–277.

Papaioannou, V., and R. Johnson. 1993. Production of chimeras and genetically defined offspring from targeted ES cells. *In* Gene Targeting: A Practical Approach. A.L. Joyner, editor. Oxford University Press, Oxford. 107–146.

Paradies, M.A., and L.M. Eisenman. 1993. Evidence of early topographic organization in the embryonic olivocerebellar projection: a model system for the study of pattern formation processes in the central nervous system. *Dev. Dyn.* 197:125–145.

Powers, J.M., and H.H. Schaumberg. 1973. The adrenal cortex of adrenoleu-

kodystrophy. *Arch. Pathol.* 96:305–310.
Powers, J.M., H.W. Moser, A.B. Moser, J.K. Upshur, B.F. Bradford, S.G. Pai, P.H. Kohn, J. Frais, and C. Tiffany. 1985. Fetal cerebrohepatorenal (Zellweger) syndrome: dysmorphic, radiologic, biochemical and pathologic findings in four affected fetuses. *Hum. Pathol.* 16:610–620.
Powers, J.M., R.C. Tummons, A.B. Moser, H.W. Moser, D.S. Huff, and R.I. Kelley. 1987. Neuronal lipidosis and neuroaxonal dystrophy in cerebrohepato-renal (Zellweger) syndrome. *Acta Neuropathol. (Berl.).* 73:333–343.
Powers, J.M., R.C. Tummons, V.C. Caviness, Jr., A.B. Moser, and H.W. Moser. 1989. Structural and chemical alterations in the cerebral maldevelopment of fetal cerebro-hepato-renal (Zellweger) syndrome. *J. Neuropathol. Exp. Neurol.* 48:270–289.
Purdue, P.E., and P.B. Lazarow. 1994. Peroxisomal biogenesis: multiple pathways of protein import. *J. Biol. Chem.* 269:30065–30068.
Rachubinski, R.A., and S. Subramani. 1995. How proteins penetrate peroxisomes. *Cell.* 83:525–528.
Rakic, P. 1972. Mode of cell migration to the superficial layers of fetal monkey neocortex. *J. Comp. Neurol.* 145:61–84.
Rakic, P. 1995. A small step for the cell, a giant leap for mankind: a hypothesis of neocortical expansion during evolution. *Trends Neurosci.* 18:383–388.
Reiner, O.R., R. Carrozzo, Y. Shen, M. Wehner, F. Faustinella, W.B. Dobyns, C.T. Caskey, and D.H. Ledbetter. 1993. Isolation of Miller-Dieker lissencephaly gene containing G-protein β-subunit-like repeats. *Nature.* 364:717–721.
Rivas, R.J., and M.E. Hatten. 1995. Motility and cytoskeletal organization of migrating cerebellar granule neurons. *J. Neurosci.* 15:981–989.
Santos, M.J., T. Imanaka, H. Shio, and P.B. Lazarow. 1987. Peroxisomal integral membrane proteins in control and Zellweger fibroblasts. *J. Biol. Chem.* 263:10502–10509.
Santos, M.J., T. Imanaka, H. Shio, G.M. Small, and P.B. Lazarow. 1988. Peroxisomal membrane ghosts in Zellweger syndrome: aberrant organelle assembly. *Science.* 239:1536–1538.
Sheppard, A.M., J.E. Brunstrom, T.N. Thornton, R.W. Gerfen, T.J. Broekelmann, J.A. McDonald, and A.L. Pearlman. 1995. Neuronal production of fibronectin in the cerebral cortex during migration and layer formation is unique to specific cortical domains. *Dev. Biol.* 172:504–518.
Shio, H., and P.B. Lazarow. 1981. Relationship between peroxisomes and endoplasmic reticulum investigated by combined catalase and glucose-6-phosphatase cytochemistry. *J. Histochem. Cytochem.* 29:1263–1272.
Shimozawa, N., T. Tsukamoto, Y. Suzuki, T. Orii, Y. Shirayoshi, T. Mori, and Y. Fujiki. 1992. A human gene responsible for Zellweger syndrome that affects peroxisome assembly. *Science.* 255:1132–1134.
Shimozawa, N., Y. Suzuki, T. Orii, A.B. Moser, H.W. Moser, and R.J.A. Wanders. 1993. Standardization of complementation grouping of peroxisome-deficient disorders and the second Zellweger patient with peroxisome assembly factor-1 (PAF-1) defect. *Am. J. Hum. Genet.* 52:843–844.
Slawecki, M.L., G. Dodt, S. Steinberg, A.B. Moser, H.W. Moser, and S.J. Gould. 1995. Identification of three distinct peroxisomal protein import defects in patients with peroxisome biogenesis disorders. *J. Cell Sci.* 108:1817–1829.
Thieringer, R., and C.R.H. Raetz. 1993. Peroxisome-deficient Chinese hamster ovary cells with point mutations in peroxisome assembly factor-1. *J. Biol. Chem.* 268:12631–12636.
Tsukamoto, T., S. Yokota, and Y. Fujiki. 1990. Isolation and characterization of chinese hamster ovary cell mutants defective in assembly of peroxisomes. *J. Cell Biol.* 110:651–660.
Tsukamoto, T., S. Miura, and Y. Fujiki. 1991. Restoration by a 35K membrane protein of peroxisome assembly in a peroxisome-deficient mammalian cell mutant. *Nature.* 350:77–81.
Volpe, J.J., and R.D. Adams. 1972. Cerebro-hepato-renal syndrome of Zellweger: an inherited disorder of neuronal migration. *Acta Neuropathol. (Berl.).* 20:175–198.
Wurst, W., and A.L. Joyner. 1993. Production of targeted embryonic stem cells. *In* Gene Targeting: A Practical Approach. A.L. Joyner, editor. Oxford University Press, New York. 33–61.
Wurst, W., A.B. Auerbach, and A.L. Joyner. 1994. Multiple developmental defects in Engrailed-1 mutant mice: an early mid-hindbrain deletion and patterning defects in forelimbs and sternum. *Development.* 120:2065–2075.
Xiang, X., A.H. Osmani, S.A. Osmani, M. Xin, and N.R. Morris. 1995. NudF, a nuclear migration gene in *Aspergillus nidulans*, is similar to the human LIS-1 gene required for neuronal migration. *Mol. Biol. Cell.* 6:297–310.
Zheng, C., H. Heintz, and M.E. Hatten. 1996. CNS gene encoding astrotactin, which supports neuronal migration along glial fibers. *Science.* 272:417–419.